








Sequential osseointegration of a novel implant system based on 3D printing in comparison with conventional titanium implants

Niklaus P. Lang^{1,2}  | Jean-Claude Imber¹  | Kiri N. Lang¹  | Bruno Schmid³  |
Fernando Muñoz⁴  | Dieter D. Bosshardt¹  | Nikola Saulacic² 

¹Department of Periodontology, School of Dental Medicine, University of Bern, Bern, Switzerland

²Department of Cranio-Maxillofacial Surgery, University Hospital, University of Bern, Bern, Switzerland

³Private Clinic ZahnArt-Belp AG, Bern, Switzerland

⁴Department of Veterinary Clinical Sciences, University of Santiago de Compostela, Lugo, Spain

Correspondence

Niklaus P. Lang, Department of Periodontology, School of Dental Medicine, University of Bern, Scheuermatweg 33, Uettligen/Bern CH-3043, Switzerland.
Email: nplangalen@gmail.com

Funding information

Ruetschi Technology (Muntelier, Switzerland)

Abstract

Objectives: To evaluate the sequential osseointegration of a novel titanium implant system based on a 3D printing technology in comparison with conventional titanium implants.

Material and methods: Two novel titanium implants based on 3D printing were tested in the mandible of eight Beagle dogs. As a control, two different commercially available titanium implants were used. The implants were staged to accommodate healing periods of 2 and 6 weeks. The primary outcome variable was bone-to-implant contact (BIC) in non-decalcified tissue sections and micro-CT analysis.

Results: Histomorphometrically, the proportions of tissues adjacent to the implant surfaces were similar for all implants, whereas the BIC percentage of new mineralized bone was greater for the control implants after both 2 and 6 weeks ($p < .05$). Micro-CT analysis revealed increasing osseous volume and BIC from 2 to 6 weeks. In contrast to the histomorphometry, the BIC evaluation with the micro-CT data revealed a significantly higher BIC for the two test implants compared with controls ($p < .001$). The analysis of the total implant surface area disclosed a value that was approximately double as high for the test compared to the control implants.

Conclusions: The novel titanium implant system based on 3D printing yielded values for osseointegration that were adequate and satisfactory. The higher percentage of new mineralized bone in the control implants is explained by the fact of a completely different three-dimensional surface area.

KEYWORDS

3D printing, histology, implant dentistry, micro-CT, osseointegration, sequential healing

1 | INTRODUCTION

In recent decades, osseointegrated dental implants have become a reliable and predictable treatment for the edentulous and partially edentulous patients (Buser et al., 2017; Rocuzzo et al., 2022). Submerged two-staged and non-submerged implants have been advocated and subsequently studied in longitudinal studies

(Cecchinato et al., 2004). Likewise, various surfaces with different texture, topography, and surface chemistry were evaluated (Buser et al., 1991; Wennerberg & Albrektsson, 2010).

More recently, implants turned out of commercially pure titanium as well as manufactured in zirconia have been promoted by various companies. While all these different implant systems were promoted by their respective manufacturers, the accurate healing

This is an open access article under the terms of the [Creative Commons Attribution-NonCommercial](https://creativecommons.org/licenses/by-nc/4.0/) License, which permits use, distribution and reproduction in any medium, provided the original work is properly cited and is not used for commercial purposes.

© 2023 The Authors. *Clinical Oral Implants Research* published by John Wiley & Sons Ltd.

with osseointegration has not been established for many systems. Sequential healing studies are only available for a few implant systems (Abrahamsson et al., 2004; Berglundh et al., 2003; Bosshardt et al., 2011; Lang et al., 2011; Rossi et al., 2014; Saulacic et al., 2012).

It is evident that sequential histological documentation should be performed prior to marketing novel implant systems. Moreover, the healing of novel implant systems should be compared with established commercially available systems that base their reputation on long-term follow-up studies.

Most recently, 3D printing has become a popular technology for manufacturing various instruments and devices (Kawaguchi et al., 2021; Ng et al., 2021; Ren et al., 2021; Spece et al., 2021; Xiu et al., 2016). Consequently, a titanium dental implant based on a 3D printing technology was developed to be applied in human jaws. The implant geometry, size, and surface texture were duplicated in the additive printing. However, no preclinical information about the healing pattern of this novel implant system is available today.

Hence, the purpose of this study was to identify the sequence of osseointegration in the 3D-printed novel titanium implant system and compare it with commercially available titanium implants.

2 | MATERIALS AND METHODS

The study protocol was submitted to and accepted by the Ethics Committee of the Rof Codina Foundation, Lugo, Spain (01/20/LU-001) following the guidelines established by the European Union Council Directive on February 1, 2013 (R.D.53/2013) using a study design that has been successfully utilized in previous studies (Araújo & Lindhe, 2009; Araújo et al., 2005; Lindhe et al., 2013). In addition, the Guidelines for Animal Research: Reporting In Vivo Experiments (Percie du Sert et al., 2020) have been included.

2.1 | Dental implants

The test groups (R1, R2) consisted of novel tissue-level, press-fit implants made of titanium alloy (Ti6Al4V, Grade 23) based on a 3D printing technology (Ø 3.3 mm/length 8 mm, Ruetschi® Technology). A trabecular structure without (R1) or with (R2) an acid pickled

surface was designed up to the polished surface, 2 mm apart from the implant shoulder (IS) (Figure S1). In addition, the control groups (R3, BLT) consisted of commercially available titanium implants. The first control implant (R3) was a screw-designed bone level implant (Ø 3.5 mm, length 8 mm, SLA surface, Ruetschi® Technology). The second control implant (BLT) was a tapered bone-level implant (Ø 3.3 mm, length 8 mm, SLActive® surface, Roxolid®, Straumann AG). Four implant types in each hemimandible were allocated according to the systematic random protocol (www.randomization.com).

2.2 | Animals

Eight female Beagle dogs with a mean age of 4.5 years were used. The animals were housed at Cebiove, Rof Codina Foundation, Lugo, Spain, with an adjusted climate (temperature: 25°C, humidity: approximately 50%, a light-dark cycle of 12:12h) and without excessive or potentially disturbing noise. Animals lived in a group kennel on concrete runs with indoor and outdoor areas, received a standard diet and water *ad libitum*. Over the entire treatment period, the dogs were monitored for their appearance, behavior, reactivity, and social interaction.

2.3 | Anesthesia

The animals were pre-anesthetized with medetomidine (10 µg/kg/i.m., Esteve) and morphine (0.4 mg/kg/i.m., Morfina Braun® 2%, B. Braun Medical). The anesthesia was initiated by propofol (2 mg/kg/i.v., Propovet®, Abbott Laboratories) and maintained by inhalation of an O₂ and 2.5%–4% isoflurane mixture (Isobavet®, Schering-Plough). Lidocaine with adrenalin (Anesvet®, Ovejero) was used for local anesthesia to reduce perioperative pain and bleeding. The sequential protocol of the surgeries is summarized in Figure 1.

2.4 | Tooth extraction

The edentulous area of three premolars and the first molars in the mandible (₂P₂, ₃P₃, ₄P₄, and ₁M₁) were selected. Sulcular incisions

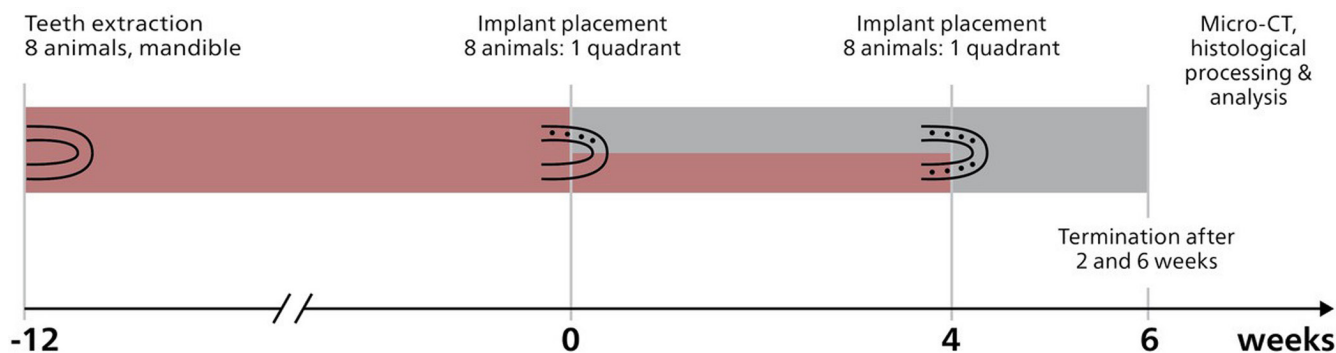


FIGURE 1 Flowsheet for clinical procedures.

were made in the premolar and molar regions, and the teeth extracted with the use of forceps and elevators following separation. The buccal and lingual flaps were replaced to close the entrance of the sockets and retained with interrupted sutures.

Postoperative pain was controlled with morphine (0.3 mg/kg/i.m./6 h, Morfina Braun 2%®, B. Braun Medical) for 24 h and meloxicam (0.1 mg/kg/s.i.d/p.o., Metacam®, Boehringer Ingelheim) for 3 days. Antibiotics (Cefovecin 8 mg/kg/s.c., Convenia®, Zoetis) were administered for 7 days. The dogs were fed a soft-pellet diet for 1 week until removal of the sutures. During the first two postoperative weeks, the oral mucosa and the teeth were disinfected three times a week by using gauzes soaked in a 0.12% chlorhexidine solution (Perio-Aid Tratamiento®, Dentaïd). Subsequently, an ultrasoft toothbrush (Perio-Aid Tratamiento®, Dentaïd) and a 0.2% chlorhexidine gel (Chlorhexidine Bioadhesive Gel, Lacer) were used for biofilm control three times per week.

2.5 | Implant installation (for 6 weeks of observation)

The healed sites were reentered after 12 weeks by a mid-crestal incision and a buccal mucoperiosteal flap elevation. Implants were placed on one side of the mandible: two test implants (R1, R2) and two conventionally produced control implants (R3, BLT). Healed sites were prepared using pilot and twist drills for all implants. The implant beds for R1 and R2 were slightly overdrilled (0.05 mm) for a press-fit implant placement. A minimum of 1 mm buccal bone thickness was preserved during site preparation. R1 and R2 implants were placed supracrestally, with the border between trabecular and machined surface positioned 1 mm subcrestally. The profile drills and taps were further used for R3 and BLT implant bed preparation. Implants shoulder was placed 1 mm subcrestally and the healing caps inserted. The flaps were repositioned and sutured for a submerged healing for all implants. Digital dental radiographs were obtained to confirm a correct position of the implants in the alveolar bone. The same postoperative protocol was followed as after tooth extraction.

2.6 | Implant installation (for 2 weeks of observation)

The healed sites were reentered 4 weeks after the first implant installation by a mid-crestal incision and a buccal mucoperiosteal flap elevation on the remaining side of the mandible. During this surgery, implants were placed for short-term observation: two test implants (R1, R2) and two control implants (R3, BLT). The same operative and postoperative protocol was followed as during the previous installation.

2.7 | Euthanasia and retrieval of specimens

Dogs were sedated with medetomidine (30 µg/kg/i.m., Esteve) and euthanised with an overdose of sodium pentobarbital (60 mg/kg/i.v.,

Dolethal, Vetoquinol). Clinical evaluation was performed, and the mandibles were retrieved by sharp dissection. The mandibles were block-sectioned using a diamond saw (Exact® Apparatebau), and bone blocks were fixed in 10% formaldehyde.

2.8 | Micro-CT analysis

Samples were scanned freshly placed in a gauze soaked in 10% formaldehyde and surrounded by a soft plastic sheet to avoid dehydration using a high-resolution micro-CT (Skyscan 1172, Bruker microCT NV). The X-ray source was set at 100 kV and 100 µA with a pixel size of 13.58 µm and the use of an aluminum/copper filter (Al 0.5). The samples were set on the object stage, and the scans were performed with a 360° rotation and images acquired every 0.4°. After the correction of the possible misalignment (smoothing = 2; beam hardening = 40; ring artifact correction = 8) of the scans, the images were reconstructed based on the Feldkamp algorithm (Feldkamp et al., 1984) using NRecon software (Bruker microCT NV) and applying the same parameters for all samples.

The reconstructed images were evaluated with the DataViewer software (Bruker microCT NV) to place implants completely parallel to the x-axis. Later, a volume of interest (VOI) of 4 mm height was delineated starting from the IS, and the transaxial view was recorded in a separate folder for the evaluation.

The transaxial images of the 4 mm VOI were loaded in CTAn software (Bruker microCT NV), and a circular VOI with the implant in the middle was selected and recorded, as previously described (Sanz-Esporrin et al., 2021). The next step in the micro-CT evaluation was the threshold selection. The threshold level was set in 80-255 for the metallic implants and 23-255 for bone-to-implant contact (BIC).

Eventually, the analysis was performed following the method described by Bruker (method note 074: "Osteintegration: Analysis of bone around a metal implant", January 2015).

The results for BV/TV in a 20-pixel region around the implant and the BIC were recorded. Additionally, the extent of the implant surface was calculated for all test (R1, R2) and control implants (R3, BLT).

2.9 | Histological preparation and analysis

The chemically fixed samples were processed into undecalcified ground sections. The specimens were rinsed in running tap water, trimmed, dehydrated in ascending concentrations of ethanol, and embedded in methylmethacrylate. The embedded tissue blocks were cut in the bucco-oral plane into approximately 600 µm thick ground sections using a slow-speed diamond saw (Varicut® VC-50, Leco). After mounting on acrylic glass slabs, the sections were ground and polished to a final thickness of about 150 µm (Knuth-Rotor-3, Struers) and surface-stained with basic fuchsin and toluidine blue/McNeal. The most central section from each implant

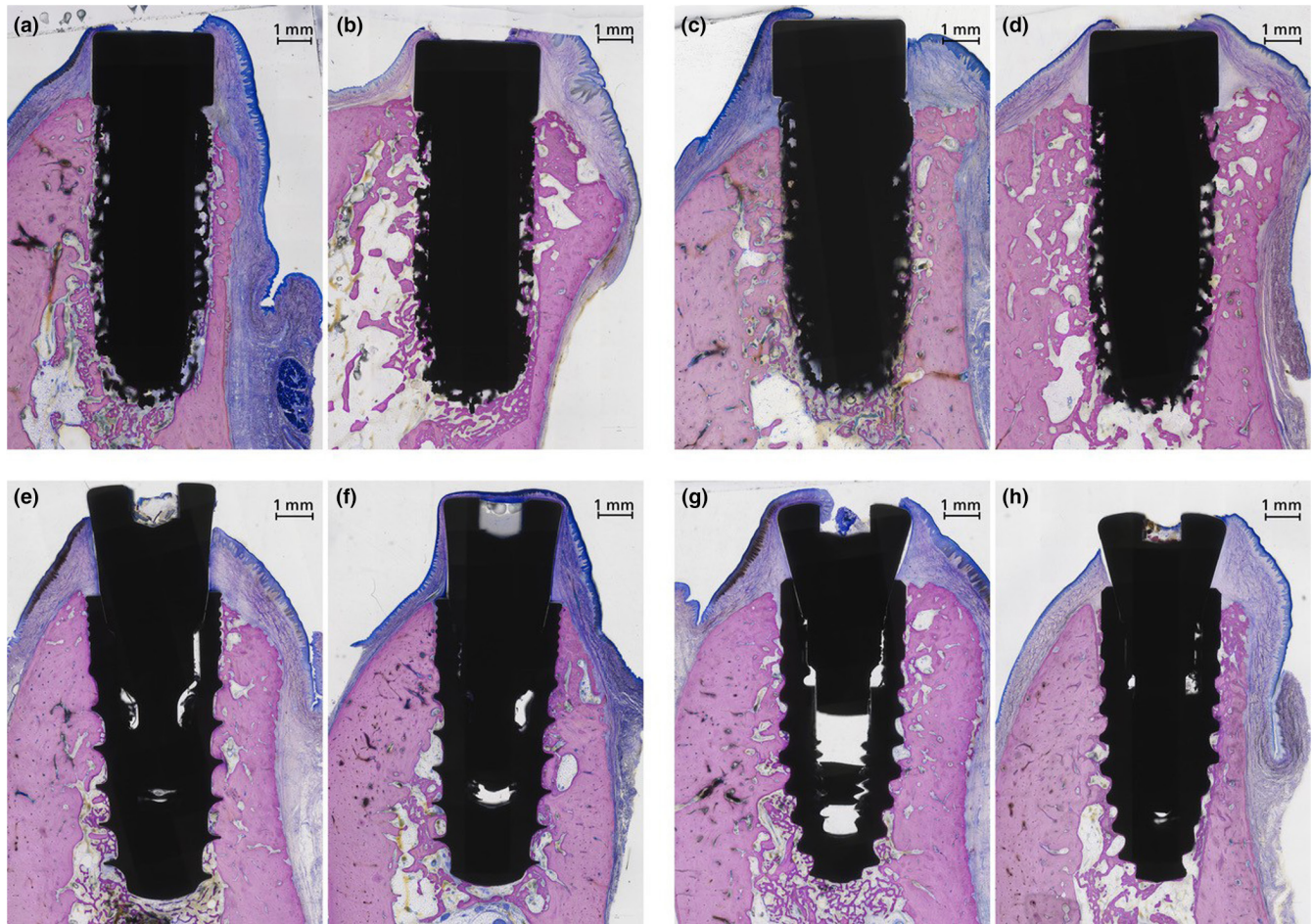


FIGURE 2 Histological documentation of the osseointegration in both test and control implants. Osseointegration of R1 after (a) 2 weeks and (b) 6 weeks. Osseointegration of R2 after (c) 2 weeks and (d) 6 weeks. Osseointegration of R3 after (e) 2 weeks and (f) 6 weeks. Osseointegration of BLT after (g) 2 weeks and (h) 6 weeks. Staining: basic fuchsin and toluidine blue/McNeal. Distance bars indicate 1 mm.

was used for descriptive and morphometric analyses. Digital photographs were taken with a digital camera (AxioCam MRC; Carl Zeiss) connected to a light microscope (Axio Imager M2; Carl Zeiss). Histo-morphometry was performed in the high-resolution digital images produced by scanning and stitching. All histo-morphometric measurements were performed on both the buccal and lingual implant surfaces.

The percentage of the following tissue areas was assessed within the first millimeter from the implant surface: osteoid, new mineralized bone, old host bone, and soft tissues.

The percentage of BIC was determined for the bone deposited along the implant surface from the first point of contact to the apical curvature at the apical contour of the implant. The percentage of the implant surface covered by osteoid, new mineralized bone, old host bone, bone debris, and soft tissues was calculated.

Linear measurements were performed from the IS (border between trabecular and polished surface for R1 and R2, and implant and healing cap for R3 and BLT) in a vertical direction using two different morphometric parameters: (1) distance from the IS to the first BIC (IS-fBIC) and (2) distance from the IS to the most coronal extension of the bone crest (IS-BC). Negative (-) values are given if IS-fBIC or

IS-BC was found apical to the IS, meaning greater bone loss for higher negative values.

As two examiners (J.C. I + K.N.L.) assessed the parameters of histo-morphometry, an interexaminer reliability test was performed by determining double measurements of eight specimens.

2.10 | Statistical analysis

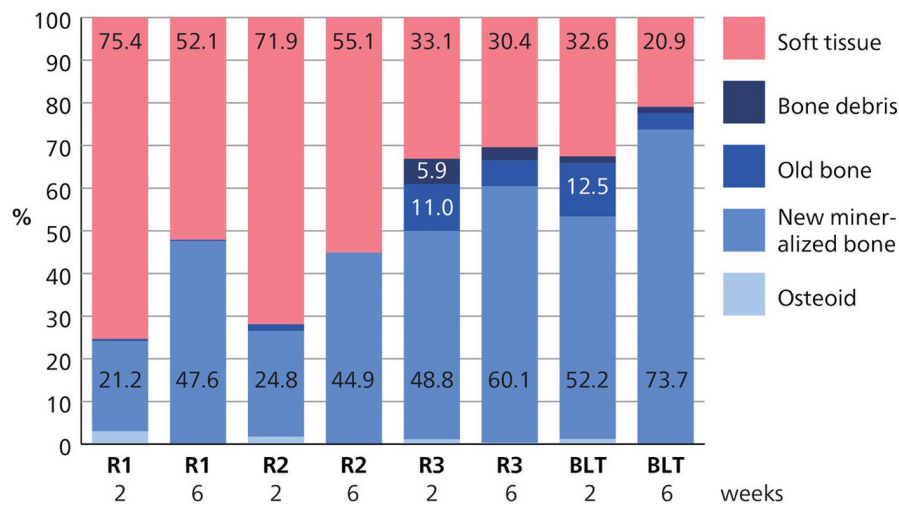
Each dog was considered as a statistical unit. Firstly, each healing time was analyzed separately to focus on the differences by group. Provided the small sample size per group (6–8 cases) a nonparametric approach was considered in the statistical analysis. Therefore, all observations were considered independent for statistical purposes. Differences in distributions of each parameter by group were tested using Kruskal–Wallis test. Pairwise comparisons were conducted using Mann–Whitney's test with *p*-value corrected by Bonferroni's criteria. Then, an overall nonparametric Brunner–Langer model was conducted to assess the main effects (group, healing time) and interaction. An ANOVA-type statistic was used in estimations. Data were described using

TABLE 1 Histometrical first bone-to-implant contact distance (mm) and bone crest distance (mm) to the implant shoulder at 2-week and 6-week observation periods in R1, R2, R3 and BLT implant groups.

	Group	Implants (n)	First BIC (mm)		Bone crest height (mm)		
			Mean	SD	Mean	SD	
2 weeks	R1	8	-0.87	0.61	-0.04	0.34	
	R2	6	-0.76	0.27	-0.05	0.31	
	R3	7	-0.71	0.50	-0.25	0.37	
	BLT	7	-1.58	0.68	-0.34	0.33	
	p-Values			R1 vs. R2	1.000	R1 vs. R2	1.000
				R1 vs. R3	1.000	R1 vs. R3	1.000
				R1 vs. BLT	0.324	R1 vs. BLT	1.000
			R2 vs. R3	1.000	R2 vs. R3	1.000	
		R2 vs. BLT	0.132	R2 vs. BLT	.606		
		R3 vs. BLT	0.156	R3 vs. BLT	1.000		
6 weeks	R1	8	-0.73	0.44	-0.21	0.35	
	R2	8	-0.45	0.37	0.05	0.49	
	R3	8	-0.48	0.30	-0.24	0.46	
	BLT	8	-0.64	0.50	-0.39	0.54	
	p-Values			R1 vs. R2	1.000	R1 vs. R2	.966
				R1 vs. R3	1.000	R1 vs. R3	1.000
				R1 vs. BLT	1.000	R1 vs. BLT	1.000
			R2 vs. R3	1.000	R2 vs. R3	.780	
		R2 vs. BLT	1.000	R2 vs. BLT	.390		
		R3 vs. BLT	1.000	R3 vs. BLT	1.000		

Note: Negative (-) values are given if the bone was apical to the implant shoulder.

Abbreviations: BIC, bone to implant contact; BLT, control implant 2; R1, test implant 1; R2, test implant 2; R3, control implant 1; SD, standard deviation.

**FIGURE 3** Bone-to-implant analysis: tissue fractions at the implant surfaces at 2 and 6 weeks for all test (R1, R2) and control (R3, BLT) implants.

means \pm standard deviation. Significance level used in analysis was set at 5% ($\alpha=.05$). An independent examiner measured parameters in a subsample of eight implants and 16 sites (buccal + lingual) in order to assess the interoperator reliability by means of intraclass correlation coefficient (ICC). ICC was estimated ≥ 0.95 .

3 | RESULTS

All implants healed without complications. No clinical infections were observed, and all animals could terminate the foreseen observation periods. The clinical observations revealed an inconspicuous

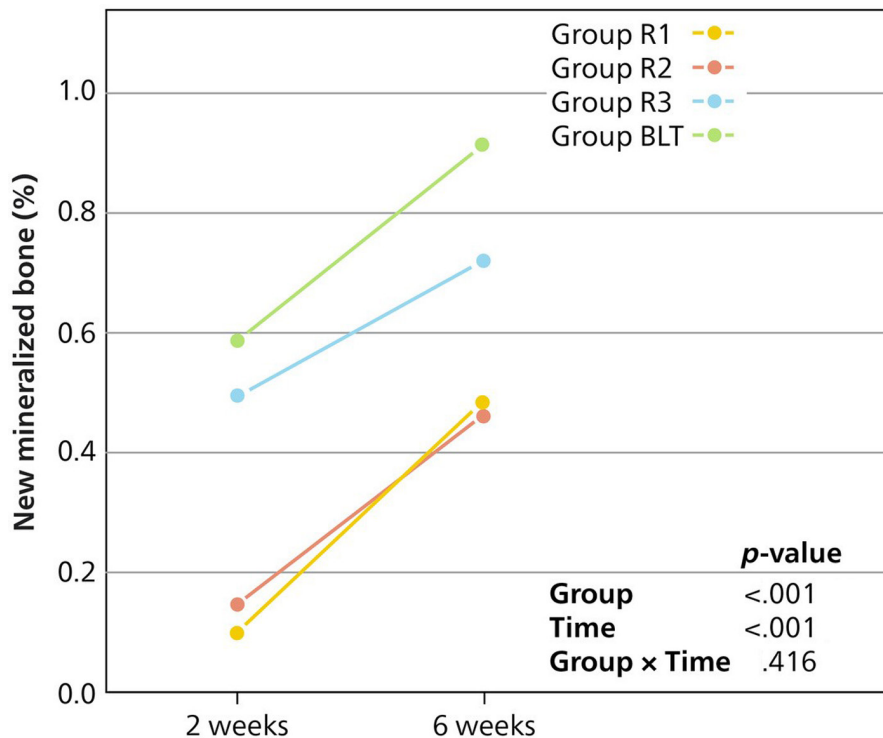


FIGURE 4 Time- and group-dependent analysis of new mineralized bone on the implant surface.

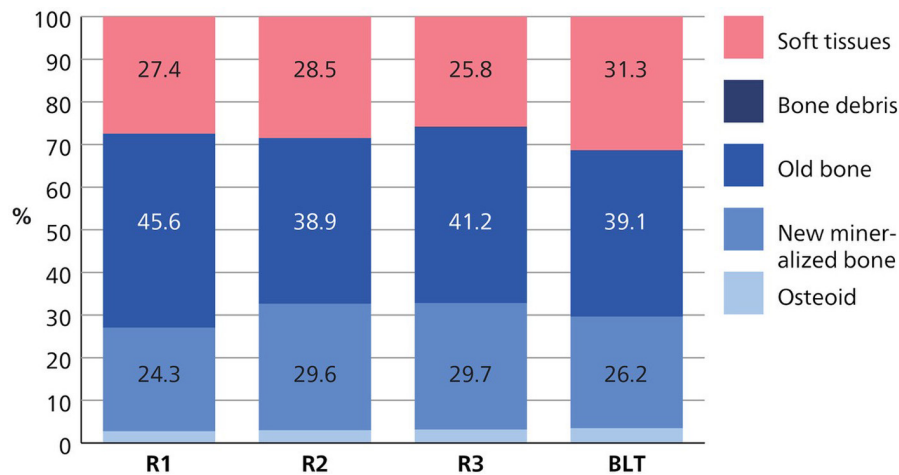


FIGURE 5 Area fraction of tissues within the first millimeter adjacent to the implant surfaces after 6 weeks for all test (R1, R2) and control (R3, BLT) implants.

healing with the absence of inflammatory signs. Digital dental radiographs after implant placement showed that all implants were located in alveolar bone in a correct position.

3.1 | Histological observations

All 64 specimens were available for descriptive analysis. For the 2 weeks' specimens, one R3 and one BLT implant showed an inflammatory infiltrate with mild pus formation. These implants originated from the same side and animal. Moreover, the R1 and R2 test implants failed to demonstrate osseointegration at this specific side and animal.

Consequently, the respective side was excluded from further analysis. Furthermore, in one R2 implant after 2 weeks, a buccal fenestration resulted in ingrowth of the mucosal connective tissue encapsulating the implant. Consequently, this specimen was excluded as well. All remaining implants after both observation periods of 2 and 6 weeks demonstrated osseointegration to various degrees (Figure 2).

3.2 | Histomorphometry

Due to the exclusions at the 2-week timepoint, 7 R1, 6 R2, 7 R3, and 7 BLT implants were evaluated. For the 6-week timepoint, all

TABLE 2 Micro-CT radiographic bone volume/tissue volume (BV/TV, %), bone-to-implant contact (BIC, %) and implant surface (mm²) at 2-week and 6-week observation periods in R1, R2, R3 and BLT implant groups.

BV/TV (%)		R1	R2	R3	BLT
2 weeks	Mean	46.331	48.5131	37.8926	39.5581
	SD	3.45287	4.97804	6.63266	7.3408
6 weeks	Mean	63.6768	65.0825	55.2275	51.8896
	SD	5.3788	5.317	10.5819	8.9823
BIC (%)		R1	R2	R3	BLT
2 weeks	Mean	59.9805	63.705	32.2422	30.8949
	SD	3.00022	5.99367	7.88958	8.5908
6 weeks	Mean	72.5262	74.9011	54.7218	50.2819
	SD	2.986	5.3566	10.6022	11.3406
Implant surface (mm ²)		R1	R2	R3	BLT
Total 2 + 6 weeks	Mean	168.5222	166.0794	89.5421	84.6341
	SD	1.15184	3.64156	0.93704	0.68798

Abbreviations: BIC, bone to implant contact; BLT, control implant 2; BV/TV, bone volume/total volume; R1, test implant 1; R2, test implant 2; R3, control implant 1; SD, standard deviation.

implants showed osseointegration without complication. Therefore, eight implants per group were analyzed.

3.3 | Vertical histomorphometry

The values for the vertical histometry are presented in [Table 1](#). The mean vertical distance (buccal + lingual) from the IS to the fBIC was smaller for both test implants compared with BLT Implants (mean: R1, -0.87 mm; R2, -0.76 mm; R3, -0.71 mm; BLT, -1.58 mm) at the 2 weeks' observation period. Yet, these differences did not reach statistical significance ($p = .324$ and $.132$, respectively). For the 6 weeks' observation period, an improvement in vertical bone remodeling was noted for all implants. Yet, no statically significant differences between the groups were revealed. The R2 implants demonstrated the smallest distance from the IS to the fBIC after 6 weeks (mean: -0.45 mm). Analyzing the bone crest height after 2 weeks did not show any statistically significant differences between the implants. However, after 6 weeks, the R2 implant revealed a higher level of the bone crest. This was true for both, the buccal and oral aspects and for the mean. Although, statistically, the level of significance to the other implants was not reached.

3.4 | Bone-to-implant contact

The BIC data are presented in [Figure 3](#) and [Table S1](#). Analyzing the BIC fractions after 2 weeks of healing revealed almost similar proportions for new mineralized bone at R1 and R2 implants (21.2% and 24.8%, respectively). The control implants R3 and BLT showed

higher proportions of new bone at this observation time (48.8% and 52.2%, respectively). The differences between the test and control implants were statistically significant ($p < .05$). The fraction of osteoid after 2 weeks was in the order of 1.2%–3.0%, without statistically significant differences between the groups. The BIC fractions after 6 weeks of integration demonstrated a statistically significant increase of new mineralized bone on the implant surface ($p < .001$) ([Figure 4](#)) reaching 47.6% and 44.9% for R1 and R2, respectively. The control groups at this time yielded 60.1% and 73.7% new mineralized bone for R3 and BLT, respectively. The time- and group-dependent increase for new mineralized bone formation was comparable for all groups ($p = .42$) ([Figure 4](#)). The control groups R3 and BLT showed statistically significantly higher values for new mineralized bone at the 6-week observation period, compared with the test groups R1 and R2 ($p < .05$).

3.5 | Area fraction

The area fraction of tissues within the first millimeter adjacent to the implant surfaces after 2 weeks was similar for all implants. After 6 weeks of incorporation, the area fraction of tissues reached, again, very similar proportions for all implants ([Figure 5](#)). Very small proportions of osteoid were noted. New mineralized bone was observed from 24.3% to 29.7%, and old bone varied between 38.9% and 45.6% ([Figure 5](#)). Bone debris was practically absent in all groups. Again, there were no statistically significant differences of any tissue fractions at any implant sites ($p > .05$). All data for the area fraction analysis are presented in [Table S2](#).

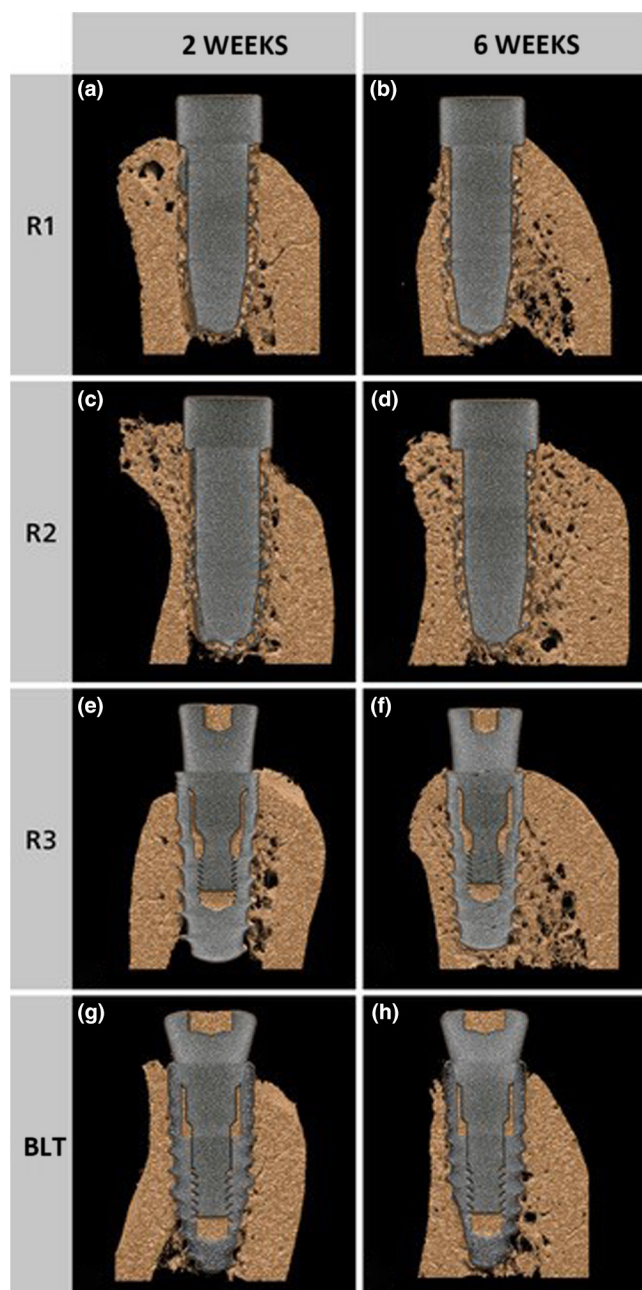


FIGURE 6 Representative radiographs from micro-CT at 2 and 6 weeks for test implants R1 (a, b) and R2 (c, d) and control implants R3 (e, f) and BLT (g, h).

3.6 | Interexaminer reliability

As two examiners assessed the parameters of histomorphometry, an interexaminer reliability test was performed by determining double measurements of eight specimens. For the proportions of tissues, for the BIC and area fraction analyses, the ICC was ≥ 0.95 for new mineralized bone and old host bone. For osteoid and bone debris fractions, the ICC was ≥ 0.75 .

3.7 | Micro-CT

The micro-CT radiographs of all the samples were reconstructed and observed from the bucco-lingual, mesio-distal, and horizontal directions. The same specimens as for the histometry were excluded for the micro-CT evaluation. The data are presented in Table 2, and representative radiographs are shown in Figure 6. From 2 to 6 weeks, osseous contact was gradually formed between the implant surface and the surrounding bone tissue without leaving a gap. At 2 weeks, a clear gap was observed between the implants and the host bone. The implant neck was in close contact with the cortical bone yielding mechanical stability. At 6 weeks, the gap between implants and the host bone was not observable anymore. In both groups of implants, a small amount of mineralized bone tissue was detected around the implants. In analyzing the parameters BV/TV and BIC (Figure 7) it is evident that the test groups, R1 and R2, yielded the best outcomes for both parameters and at both observation periods. The BV/TV reached a mean of 46.3% and 48.5% after 2 weeks and 63.7 and 65.1 after 6 weeks for R1 and R2, respectively. This was statistically significantly better than the BV/TV recorded at the two control implants ($p < .05$). The test implants with the acid pickled surface (R2) demonstrated the highest amount of BIC of 74.9% after 6 weeks, while the test implant without acid pickling (R1) had a 6-week BIC of 72.5%. The R3 implants displayed a 6-week BIC of 54.7%. This was not statistically significantly different from the BLT implant value (50.3%) but reached the statistical significance when comparing with the two 3D-printed implants (R1, R2, $p < .05$). The calculation of the extent of the implant surfaces was 168.5 and 166.1 mm² for R1 and R2, respectively. These values were significantly higher ($p < .001$) than those for the R3 and BLT implants (R3: 89.5 mm²; BLT: 84.6 mm²).

4 | DISCUSSION

The present study has been designed to evaluate the process of osseointegration for an implant system manufactured with a novel technology of 3D printing and hereby comparing this biological process with that known for moderately rough titanium implant surfaces.

The results of the new 3D-printed devices were affected by the surface structure (example for R2 see Figure 8). Consequently, the interpretation of the osseointegration process has to consider these differences of surface topography. The osseointegration of conventional implants is well studied and generally, the bone-to-implant contact (BIC %) as a primary outcome variable was used (Berglundh et al., 2003). In the present study, the values obtained in BIC percentages after 2 and 6 weeks corresponded to those described earlier (Berglundh et al., 2003). Both, the R3 and BLT implants yielded similar BIC percentages after the respective observation periods (52.2% and 48.8% after 2 weeks, respectively

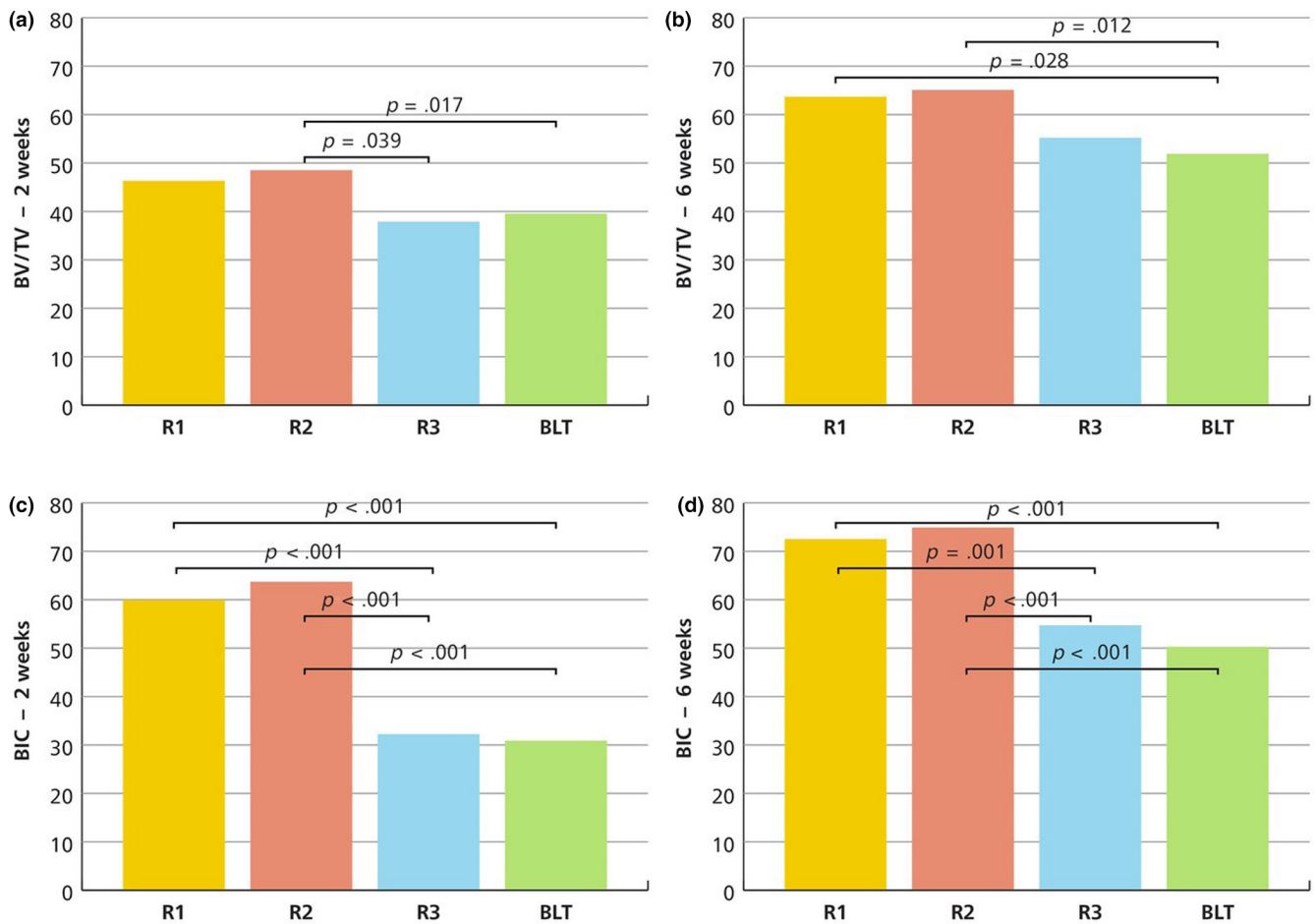


FIGURE 7 Micro-CT analysis: bone volume (BV)/ total volume (TV) after (a) 2 weeks and (b) 6 weeks. Bone-to-implant contact (BIC) after (c) 2 weeks and (d) 6 weeks.

and 73.7% and 60.1% after 6 weeks, respectively). Hence, these conventional implants truly represented a control to which the osseointegration process of the novel 3D-printed devices may be compared. It has to be kept in mind, however, that BIC on conventional implants is measured on a linear outline of the implant surfaces incorporated into bone, while the same parameter is not generated with the same methodology in the 3D-printed devices, as the outline of the implant surface does not follow a simple line but represents a 3D network of a trabecular structure projected on a 2D plane (Figure 8). This, in turn, means that the total surface available for the osseointegration process is higher, as shown by a statistically significantly higher surface area for the test implants compared with the control implants ($p < .001$). In the latter, the test implants disclosed a surface area that was approximately double as high than that available for the control implants. Hence, the new mineralized bone formation occupied a larger volume that requires more healing time than in conventional implant designs. Moreover, the total surface covered with new bone in a 3D-printed device may represent a higher absolute bone volume covering the implant surface, even though the percentage of new mineralized bone on the implant surface is reduced in comparison with the conventional implants.

In the present study, the percentages of new mineralized bone were significantly lower for R1 and R2 (21.2% and 24.8% after 2 weeks, and 47.6% and 44.9% after 6 weeks, respectively) compared with R3 and BLT. Yet, such percentages indicate successful osseointegration, although the values were lower than those for the SLA surfaces. They corresponded to the osseointegration of turned titanium surfaces after 2 and 6 weeks in the Beagle dog model (Abrahamsson et al., 2004). In a human biopsy model (Lang et al., 2011), the osseointegration process reached approximately 15% of new mineralized bone on the implant surface after 2% and 62% after 6 weeks, respectively. Obviously, the direct bone formation on the 3D-printed implant surfaces is by far adequate for functional stability. However, only a study on loaded 3D-printed implants would give the definite proof of such a statement.

The analysis of the data of micro-CT in the present study did not correspond with those obtained by histomorphometry. In the micro-CT analysis, the R1 and R2 implants yielded superior outcomes compared with R3 and BLT in terms of BIC, while, in the histomorphometry, these parameters showed a reversed result. Again, the discrepancy of the BIC data can be explained on the basis of methodology and the surface morphology by the 3D printing procedure. Such discrepancies between the two methods

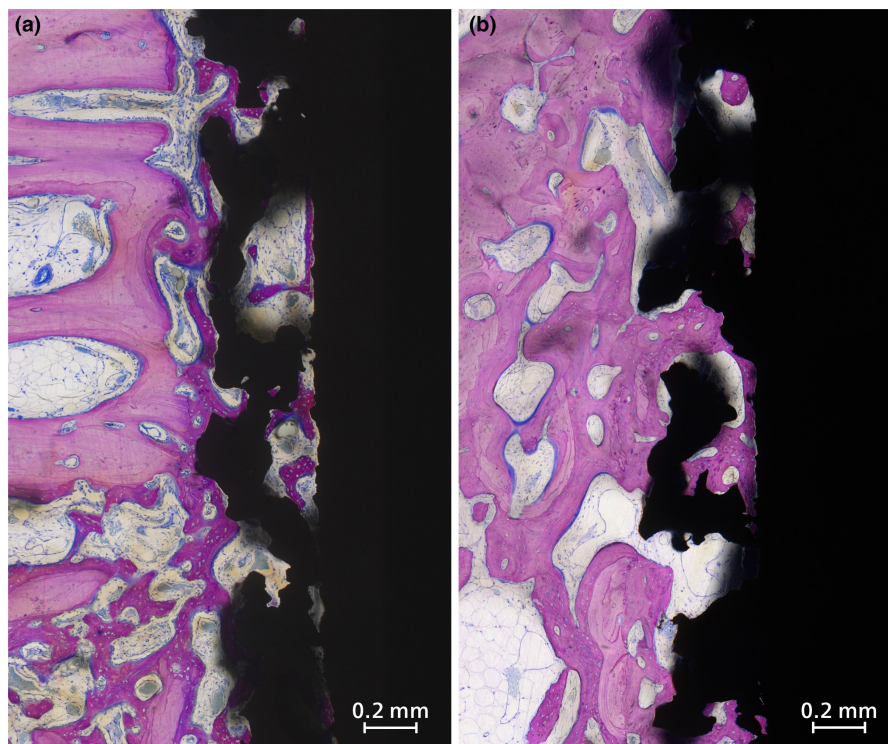


FIGURE 8 Surface topography of a R2 implant after (a) 2 weeks and (b) 6 weeks after implant installation. Staining: basic fuchsin and toluidine blue/McNeal. Distance bars indicate 0.2 mm.

are rarely discussed in the literature. Obviously, micro-CT data do not reliably reflect the BIC as determined by the standard of histology. As the histological sections are more suitable to distinguish cells, nonmineralized osteoid and soft tissue, the micro-CT is appropriate to analyze the mineralized tissue during later periods of healing (Nakahara et al., 2020). Nevertheless, the BV/TV parameter appeared to be similar in the micro-CT if compared with the area fraction analysis in histomorphometry. Moreover, it has to be realized that the micro-CT technology is not able to distinguish between osteoid, new mineralized bone, and old bone. Also, bone debris cannot be identified. Micro-CT is also not able to detect peri-implant inflammation/infection (two implants were excluded from the histomorphometric analyses based on histologic detection of infection). Hence, it appears as a necessity to study the osseointegration process with histomorphometry.

Analyzing the bone levels after 2 and 6 weeks following the incorporation of the implants indicated a superior level of crestal bone with the R1 and R2 implants compared with the controls (R3, BLT). However, this superiority did not reach statistical significance most likely owing to the limited number of experimental animals used in the present study. The increased crestal bone levels may indicate that the novel 3D-printed devices do not exercise pressure to the adjacent bone after placement and hence, bone levels may most likely be preserved. Nevertheless, other dissimilarities between the implant design including presence of the micro-gap or possibility of platform switching might have affected the results.

In the present study, the Beagle dog model was chosen because of the feasibility and the established, well-controlled animal facility

in Lugo, Spain. Despite the superb and competent animal care rendered, the histological analysis showed that in one dog, an obvious site infection developed. This happened for two implants on the same side of the mandible. Consequently, that side (four implants) was eliminated from further analysis, reducing the number of estimates. Furthermore, one implant in another dog demonstrated a buccal fenestration with concomitant ingrowth of soft tissue. This single implant also was excluded from further analysis. All other 59 implants were placed in adequate volumes of bone and in the right positions. Evaluating these shortcomings, it has to be stated that the experiment could be performed with clinical accuracy, and the osseointegration resulted in undisturbed healing and implant stability.

The application of different fabrication technologies and trabecular implant surface represents a limitation of the present study. 3D-printed titanium dental implants have microscopic structures highly dissimilar to those of traditional milled-titanium implants, which have still not been comprehensively evaluated. A significant alteration of a surface topography observed after 3D printing fabrication is believed to possess better biocompatibility and osseointegration ability than the commercial titanium implants. 3D-printed mesh implant induced a higher wettability formation that caused an easier liquid flow into the gaps and formation of a hydrophilic interface, which in turn affects the surface biocompatibility (Huang et al., 2019). In vitro cell behavior and the biosafety assays of 3D-printed implants and plates were comparable or even likely improved as compared with that of conventionally fabricated titanium (Wang et al., 2023; Yang et al., 2017).

Significantly thicker native TiO₂ layer formed on the 3D-printed mesh surface shell impede the metallic ions to leach out and enhance the wear and corrosion resistance (Huang et al., 2019). The study of Ng et al. (2021) further confirmed that the 3D-printed titanium-alloy Grade 23 implants should be considered as safe as the standard milled implants in terms of serum and organ titanium levels. If wear and corrosion would be increased in load-bearing 3D-printed implants with different surface morphologies should be demonstrated in a later tribology study.

From a clinical point of view, it was important to get information on the early healing phase of osseointegration with this novel 3D-printed implant system. Obviously, the BIC fractions obtained after 2 weeks were of a magnitude that would allow implant stability for further osseointegration in the weeks to come. After 6 weeks, the BIC fractions were at least as high as known from traditional implant systems with turned surfaces. Hence, the suitability of the 3D-printed devices for oral reconstructions is a given fact. It remains to be demonstrated to what extent implant stability is guaranteed in the long term. Furthermore, the process of disintegration of 3D-printed implants as a result of a peri-implant infection has to be addressed in further studies.

In summary, titanium implants manufactured by the technology of 3D printing have been shown to successfully osseointegrate with adequate fractions of new mineralized bone formation after 2 and 6 weeks. The crestal bone height appears to be maintained in an optimal way when compared with conventional implant systems.

AUTHOR CONTRIBUTIONS

Conception, planning, supervision, and manuscript drafting: Niklaus P. Lang. Histomorphometric analysis, data collection, statistics, and manuscript drafting: Jean-Claude Imber. Histomorphometric analysis, data collection, and manuscript approval: Kiri N. Lang. Surgical planing and procedures, manuscript approval: Bruno Schmid. Micro-CT analysis, data collection, veterinary supervision, and manuscript approval: Fernando Muñoz. Histomorphometric analysis, data interpretation, and manuscript approval: Dieter D. Bosshardt. Conception, surgical planing and procedures, statistics, and manuscript drafting: Nikola Saulacic.

ACKNOWLEDGMENTS

This study was supported by Ruetschi Technology (Muntelier, Switzerland). The cooperation with Christoph Ruetschi, Bastien Boillat, and David Chenaux is highly appreciated. The competent animal care of the Veterinary Faculty Lugo, University of Santiago de Compostela, Lugo, España, and the technical assistance of the micro-CT analysis by Dr. María Permuy Mendaña is highly acknowledged and appreciated. The staff and Faculty of the Robert K. Schenk Laboratory of Oral Histology, University of Bern contributed substantially to the histological analysis in the present paper. Especially, Silvia Owusu is given credit for her competent guidance. Open access funding provided by Universitat Bern.

FUNDING INFORMATION

This study has been funded in full by Ruetschi Technology SA, Muntelier, Switzerland.

CONFLICT OF INTEREST STATEMENT

The authors declare no conflict of interest with the present study or the sponsoring company.

DATA AVAILABILITY STATEMENT

The data that support the findings of this study are available from the corresponding author upon reasonable request.

ETHICS STATEMENT

The study protocol was submitted to and approved by the Ethics Committee for Animal Research at the Rof Codina Foundation (01/20/LU-001), following the guidelines established by the European Union Council Directive on February 1, 2013 (R.D.53/2013). In addition, the Guidelines for Animal Research: Reporting In Vivo Experiments (ARRIVE) have been followed.

ORCID

Niklaus P. Lang  <https://orcid.org/0000-0002-6938-9611>

Jean-Claude Imber  <https://orcid.org/0000-0001-6690-5249>

Kiri N. Lang  <https://orcid.org/0000-0002-3461-7418>

Bruno Schmid  <https://orcid.org/0000-0002-9676-8879>

Fernando Muñoz  <https://orcid.org/0000-0002-4130-1526>

Dieter D. Bosshardt  <https://orcid.org/0000-0002-2132-6363>

Nikola Saulacic  <https://orcid.org/0000-0003-3960-4920>

REFERENCES

- Abrahamsson, I., Berglundh, T., Linder, E., Lang, N. P., & Lindhe, J. (2004). Early bone formation adjacent to rough and turned endosseous implant surfaces. An experimental study in the dog. *Clinical Oral Implants Research*, 15(4), 381–392. <https://doi.org/10.1111/j.1600-0501.2004.01082.x>
- Araújo, M. G., & Lindhe, J. (2009). Ridge alterations following tooth extraction with and without flap elevation: An experimental study in the dog. *Clinical Oral Implants Research*, 20(6), 545–549. <https://doi.org/10.1111/j.1600-0501.2008.01703.x>
- Araújo, M. G., Sukekava, F., Wennström, J. L., & Lindhe, J. (2005). Ridge alterations following implant placement in fresh extraction sockets: An experimental study in the dog. *Journal of Clinical Periodontology*, 32(6), 645–652. <https://doi.org/10.1111/j.1600-051X.2005.00726.x>
- Berglundh, T., Abrahamsson, I., Lang, N. P., & Lindhe, J. (2003). De novo alveolar bone formation adjacent to endosseous implants. *Clinical Oral Implants Research*, 14(3), 251–262. <https://doi.org/10.1034/j.1600-0501.2003.00972.x>
- Bosshardt, D. D., Salvi, G. E., Huynh-Ba, G., Ivanovski, S., Donos, N., & Lang, N. P. (2011). The role of bone debris in early healing adjacent to hydrophilic and hydrophobic implant surfaces in man. *Clinical Oral Implants Research*, 22(4), 357–364. <https://doi.org/10.1111/j.1600-0501.2010.02107.x>
- Buser, D., Schenk, R. K., Steinemann, S., Fiorellini, J. P., Fox, C. H., & Stich, H. (1991). Influence of surface characteristics on bone integration of titanium implants. A histomorphometric study in miniature pigs. *Journal of Biomedical Materials Research*, 25(7), 889–902. <https://doi.org/10.1002/jbm.820250708>
- Buser, D., Sennerby, L., & De Bruyn, H. (2017). Modern implant dentistry based on osseointegration: 50 years of progress, current trends and open questions. *Periodontology 2000*, 73(1), 7–21. <https://doi.org/10.1111/prd.12185>
- Cecchinato, D., Olsson, C., & Lindhe, J. (2004). Submerged or non-submerged healing of endosseous implants to be used in the rehabilitation of

- partially dentate patients. *Journal of Clinical Periodontology*, 31(4), 299–308. <https://doi.org/10.1111/j.1600-051X.2004.00527.x>
- Feldkamp, L. A., Davis, L. C., & Kress, J. W. (1984). Practical cone-beam algorithm. *Journal of the Optical Society of America A*, 1(6), 612–619. <https://doi.org/10.1364/JOSAA.1.000612>
- Huang, M. T., Juan, P. K., Chen, S. Y., Wu, C. J., Wen, S. C., Cho, Y. C., Huang, M. S., Chou, H. H., & Ou, K. L. (2019). The potential of the three-dimensional printed titanium mesh implant for cranioplasty surgery applications: Biomechanical behaviors and surface properties. *Materials Science & Engineering. C, Materials for Biological Applications*, 97, 412–419. <https://doi.org/10.1016/j.msec.2018.11.075>
- Kawaguchi, M., Segawa, A., Shintani, K., Nakamura, Y., Ishigaki, Y., Yonezawa, K., Sasamoto, T., Kaneuji, A., & Kawahara, N. (2021). Bone formation at Ti-6Al-7Nb scaffolds consisting of 3D honeycomb frame and diamond-like carbon coating implanted into the femur of beagles. *Journal of Biomedical Materials Research. Part B, Applied Biomaterials*, 109(9), 1283–1291. <https://doi.org/10.1002/jbm.b.34789>
- Lang, N. P., Salvi, G. E., Huynh-Ba, G., Ivanovski, S., Donos, N., & Bosshardt, D. D. (2011). Early osseointegration to hydrophilic and hydrophobic implant surfaces in humans. *Clinical Oral Implants Research*, 22(4), 349–356. <https://doi.org/10.1111/j.1600-0501.2011.02172.x>
- Lindhe, J., Araújo, M. G., Bufler, M., & Liljenberg, B. (2013). Biphasic alloplastic graft used to preserve the dimension of the edentulous ridge: An experimental study in the dog. *Clinical Oral Implants Research*, 24(10), 1158–1163. <https://doi.org/10.1111/j.1600-0501.2012.02527.x>
- Nakahara, K., Haga-Tsujimura, M., Igarashi, K., Kobayashi, E., Schaller, B., Lang, N. P., & Saulacic, N. (2020). Single-staged implant placement using the bone ring technique with and without membrane placement: Micro-CT analysis in a preclinical in vivo study. *Clinical Oral Implants Research*, 31(1), 29–36. <https://doi.org/10.1111/clr.13543>
- Ng, S. L., Das, S., Ting, Y. P., Wong, R. C. W., & Chanchareonsook, N. (2021). Benefits and biosafety of use of 3D-printing technology for titanium biomedical implants: A pilot study in the rabbit model. *International Journal of Molecular Sciences*, 22(16), 8480. <https://doi.org/10.3390/ijms22168480>
- Percie du Sert, N., Hurst, V., Ahluwalia, A., Alam, S., Avey, M. T., Baker, M., Browne, W. J., Clark, A., Cuthill, I. C., Dirnagl, U., Emerson, M., Garner, P., Holgate, S. T., Howells, D. W., Karp, N. A., Lazic, S. E., Lidster, K., MacCallum, C. J., Macleod, M., ... Würbel, H. (2020). The ARRIVE guidelines 2.0: Updated guidelines for reporting animal research. *PLoS Biology*, 18(7), e3000410. <https://doi.org/10.1371/journal.pbio.3000410>
- Ren, B., Wan, Y., Liu, C., Wang, H., Yu, M., Zhang, X., & Huang, Y. (2021). Improved osseointegration of 3D printed Ti-6Al-4V implant with a hierarchical micro/nano surface topography: An in vitro and in vivo study. *Materials Science & Engineering. C, Materials for Biological Applications*, 118, 111505. <https://doi.org/10.1016/j.msec.2020.111505>
- Rocuzzo, A., Imber, J. C., Marruganti, C., Salvi, G. E., Ramieri, G., & Rocuzzo, M. (2022). Clinical outcomes of dental implants in patients with and without history of periodontitis: A 20-year prospective study. *Journal of Clinical Periodontology*, 49, 1346–1356. <https://doi.org/10.1111/jcpe.13716>
- Rossi, F., Lang, N. P., De Santis, E., Morelli, F., Favero, G., & Botticelli, D. (2014). Bone-healing pattern at the surface of titanium implants: An experimental study in the dog. *Clinical Oral Implants Research*, 25(1), 124–131. <https://doi.org/10.1111/clr.12097>
- Sanz-Esporrin, J., Di Raimondo, R., Vignoletti, F., Núñez, J., Muñoz, F., & Sanz, M. (2021). De novo bone formation around implants with a surface based on a monolayer of multi-phosphonate molecules. An experimental in vivo investigation. *Clinical Oral Implants Research*, 32(9), 1085–1096. <https://doi.org/10.1111/clr.13803>
- Saulacic, N., Bosshardt, D. D., Bornstein, M. M., Berner, S., & Buser, D. (2012). Bone apposition to a titanium-zirconium alloy implant, as compared to two other titanium-containing implants. *European Cells & Materials*, 23, 273–286. <https://doi.org/10.22203/ecm.v023a21>
- Spece, H., Basgul, C., Andrews, C. E., MacDonald, D. W., Taheri, M. L., & Kurtz, S. M. (2021). A systematic review of preclinical in vivo testing of 3D printed porous Ti6Al4V for orthopedic applications, part I: Animal models and bone ingrowth outcome measures. *Journal of Biomedical Materials Research. Part B, Applied Biomaterials*, 109(10), 1436–1454. <https://doi.org/10.1002/jbm.b.34803>
- Wang, Q., Telha, W., Wu, Y., Abotaleb, B., Jiang, N., & Zhu, S. (2023). Evaluation of the properties of 3D-printed ti alloy plates: In vivo and in vitro comparative experimental study. *Journal of Clinical Medicine*, 12(2), 444. <https://doi.org/10.3390/jcm12020444>
- Wennerberg, A., & Albrektsson, T. (2010). On implant surfaces: A review of current knowledge and opinions. *The International Journal of Oral & Maxillofacial Implants*, 25(1), 63–74.
- Xiu, P., Jia, Z., Lv, J., Yin, C., Cheng, Y., Zhang, K., Song, C., Leng, H., Zheng, Y., Cai, H., & Liu, Z. (2016). Tailored surface treatment of 3D printed Porous Ti6Al4V by microarc oxidation for enhanced osseointegration via optimized bone in-growth patterns and interlocked bone/implant interface. *ACS Applied Materials & Interfaces*, 8(28), 17964–17975. <https://doi.org/10.1021/acsami.6b05893>
- Yang, F., Chen, C., Zhou, Q., Gong, Y., Li, R., Li, C., Klämpfl, F., Freund, S., Wu, X., Sun, Y., & Yu, Y. (2017). Laser beam melting 3D printing of Ti6Al4V based porous structured dental implants: Fabrication, biocompatibility analysis and photoelastic study. *Scientific Reports*, 7, 45360. <https://doi.org/10.1038/srep45360>

SUPPORTING INFORMATION

Additional supporting information can be found online in the Supporting Information section at the end of this article.

How to cite this article: Lang, N. P., Imber, J.-C., Lang, K. N., Schmid, B., Muñoz, F., Bosshardt, D. D., & Saulacic, N. (2023). Sequential osseointegration of a novel implant system based on 3D printing in comparison with conventional titanium implants. *Clinical Oral Implants Research*, 34, 627–638. <https://doi.org/10.1111/clr.14072>